Int. J. Electrochem. Sci., 15 (**2020**) 7709 – 7721, doi: 10.20964/2020.08.80

International Journal of
ELECTROCHEMICAL
SCIENCE
www.electrochemsci.org

Electrochemical Controlled Synthesis of Au/Ni Nano-arrays and its Sintering with Ag NPs Paste

Zhen Zheng[1], *Fan Yang*[1], *Wei Liu*[1,*], *Fanyu Meng*[2], *Rong An*[1,3], *Wei Zhang*[1], *Haibo Wang*[1], *Yiping Wang*[1], *Chunqing Wang*[1,3,*]

[1] State Key Laboratory of Advanced Welding and Joining, Harbin Institute of Technology, Harbin 150001, China
[2] Department of Environmental Hygiene, School of Public Health, Harbin Medical University, Harbin 150081, China
[3] Key Laboratory of Micro-systems and Micro-structures Manufacturing, Ministry of Education, Harbin Institute of Technology, Harbin 150080, China
[*]E-mail: w_liu@hit.edu.cn, wangcq@hit.edu.cn

Received: 8 March 2019 / *Accepted:* 18 June 2020 / *Published:* 10 July 2020

The microstructure gap between the nanopaste and the conventional pad led to the high practical connection temperature. In this paper, we focused on the preparation of the different microstrucutre Ni nanocone arrays and their sintering behaviors. The electrochemical behavior of ethylenediamine hydrochloride (EDH) on the Ni deposition was studied. The SEM, XRD, linear polarization and impedance spectroscopy analysis results showed that EDH could facilitate the oriented growth of nickel and decrease the polarization of electrodeposition. Different Ni nanocone arrays were prepared by tuning the EDH concentration, current density and solution temperature. The pads coated with Ni/Au nanocone arrays were connected with Ag NPs paste. The shear test result showed that the surface array microstructure played a significant role in enhancing the joint strength. When the nanocone bottom diameter was 150 nm, the joint hold the best shear strength.

Keywords: Ni nanocone arrays, Ethylenediamine hydrochloride, Ag NPs, Sinter, Shear strength

1. INTRODUCTION

The miniaturization and integration are the developed trend in the power device field. Due to the increasing power density, the power devices are supposed to operate at high temperature and be applied in harsh environments such as aerospace exploration and deep well detection. Compared with Si, the new generation semiconductor SiC possesses higher breakdown voltage, electron mobility and operating temperature, which make it a promising alternative in high power electronics [1-3]. However, traditional die-attach materials cannot meet the high temperature service requirement. The Pb, Au and Zn based

solders could be served at high temperature, while they have other problems, such as toxicity, high cost, bad corrosion resistance and brittleness [4-6]. Besides, the bulk solders usually need to remelt at high temperature to form the reliable joint, which may damage the thermosensitive components. Therefore, it is imperative to develop the new interconnecting material to meet the high temperature service demand.

Nano material connection property has attracted substantial attentions in the electronic packaging field. Due to the nano-size effect, nano materials could be sintered at much lower temperature than their melt point. Once the nano materials sinter finished, the nano material joint would revert to the bulk material property. The nano materials offer a possibility to connect at low temperature and serve at high temperature. Depend on their special sinter property, nano materials are becoming potential alternatives in die-attach materials such as Ag nanoparticle (NP) paste, Cu NP paste, Ag/Cu alloy NP paste and Cu_6Sn_5 NP paste [7-10]. And the Ag NP paste has been intended to apply in some electronic packaging process based on the good joint shear strength, heat and electrical conductivity [11, 12].

It was found the nano-particle paste sinter process contained two steps. In the first sinter step, due to the nano-particle high surface energy, nano-particles spontaneously sintered together in a short time and formed the bigger and more stable particles [13]. And then in the next step, the nano- or even micro- particles formed in the first step started to connect with the pad; this step was the inter-diffusion between the bigger particles and the pad. The second step needed longer time to finish the effective connection. Due to the large microstructure gap between nano-paste and macro pad, the sintering behaviors between them needed higher sinter temperature, and the sinter efficiency was usually lower. Our prior work showed the pad surface nanostructure (Ni nanocone arrays) could promote the sinter between the nano-particle paste and the pad, which could reduce two sinter steps to one step [14]. The surface nanostructure could narrow the surface energy/chemical potential gap between nanoparticles and pad surface, and it was possible to achieve the competitive relationship between nanoparticles self-sinter and paste-pad sinter and improve the nano-paste sinter compatibility.

It was confirmed the surface array microstructure played a vital role in the nano-paste sinter process. In order to fabricate the appropriate nanostructure to enhance the joint, the electrochemical parameter effects and the formation mechanism of Ni nano array need to be studied. In this paper, the formation mechanism of Ni nano array was studied by electrochemical tests and XRD characterization. The different Ni nano arrays were deposited by tuning the electroplating parameters. The joint sintered between the pad coated by Ni/Au nano array and Ag NP paste exhibited the excellent mechanical property.

2. EXPERIMENT

2.1. Fabrication of Ni Nanocone Arrays

All reagents were of analytical pure grade and used as received without further purification. The copper pad (99.95 %, 20 mm × 30 mm × 2 mm) was selected as cathode. Before electrodeposition, the Cu pad was immersed into 5 wt.% NaOH aqueous solution and 10 wt.% HNO_3 aqueous solution to

remove the grease and oxide on the surface respectively. After that, the sample was washed by deionized water twice and dried by the cool air. Ni plate, commercial pure (99.9 %), was chosen as anode material. The plating bath was composed of $NiCl_2 \cdot 6H_2O$ (200 g L^{-1}), H_3BO_3 (25 g L^{-1}) and EDH. The Ni normal layer deposited on the Cu pad from the plating solution without EDH was the control group. Besides, HCl and $NH_3 \cdot H_2O$ were employed to adjust pH value. After electroplating, the substrate was rinsed by deionized water and then dried by cool air.

2.2. Electroless Gold Plating

The substrate with Ni nano array was ultrasonically cleaned in ethanol to dissolve the organics absorbed on the Ni nanocone array surface. The substrate was totally immersed in the electroless Au solution, which was composed of $Na_3Au(SO_3)_2$ (2 g L^{-1}) and Na_2SO_3 (36.8 g L^{-1}). The solution was kept at 80 °C under vigorous stirring condition. Finally, the sample was washed by deionized water and ethanol solution, and then dried by cool air.

2.3. Preparation of Ag NP Paste

Ag NPs were synthesized by Li group's method [15]. Solution A contained Na_3citrate$\cdot 2H_2O$ solution (400 g L^{-1}) and $FeSO_4 \cdot 7H_2O$ solution (300 g L^{-1}), the ratio was 7:5. Solution B was $AgNO_3$ solution (100 g L^{-1}). Solution A was dropped in the solution B slowly with vigorous stirring. When the reaction finished, the suspension was centrifuged at 3000 rpm for 5 min, the supernatant was abandoned and the precipitate was Ag NP paste. The Ag NP paste was stored under 0 °C.

2.4. Sinter Joint Preparation

Both the dummy die and substrate were Ni/Au nano array coated copper plates. The square layer of Ag NP paste was screen printed on the substrate and the paste thickness was 20 ± 1 μm. Then the die was picked and placed on the Ag NP paste layer to form the sandwiched sample. The sample was directly heated in an oven up to 250 °C in air atmosphere, and held for 30 min. The heating rate was 5 °C min^{-1} from ambient temperature. Finally, the sample was naturally cooled to room temperature and collected for the following test.

2.5. Electrochemical Test

Electrochemical Workstation (CHI 760E) was employed to accomplish linear polarization and impedance spectroscopy analysis. Electrochemical tests were both carried out in the three-electrode system, the copper plate (99.95 %, diameter 1 cm), platinum plate (99.99 %) and saturated calomel electrode (SCE) were selected as working electrode, auxiliary electrode and reference electrode respectively. The electrolyte ($NiCl_2 \cdot 6H_2O$ 200 g L^{-1}, H_3BO_3 25 g L^{-1}) with different EDH concentrations were kept at 65 °C. In linear polarization analysis, the scanning rate was 1 mV s^{-1}. In impedance

spectroscopy analysis, the overpotential was set as 250 mV. Electrochemical impedance measurements were recorded in the 0.1 Hz - 10 kHz frequency range using a 10 mV AC perturbation at 65 °C.

2.6. Microstructure Characterization and Shear Strength

The sample crystalline structure was characterized by X-ray diffraction (XRD; Empyrean, Cu Kα). Scanning electron microscopy (SEM; FEI, Helios NanoLab 600i) was conducted to observe the surface morphology of the Ni array on the pad. Transmission electron microscopy was used to observe Ag NPs' morphology. The die shear tester (Dage 4000) was used to test the shear strength of sintered sample. The shear height and speed were 50 μm and 200 μm s^{-1} respectively.

3. RESULTS AND DISSCUSSION

3.1. EDH Effect on Morphology and Crystal Growth

EDH was supposed to play a vital role in the Ni nanoarrays oriented growth. SEM was conducted to observe the morphologies of Ni film formed with different EDH concentrations, which was set as 0, 0.3, 0.6, 0.9, 1.2 and 1.5 mol L^{-1} respectively. The electroplating current density and solution temperature were set as 2 A dm^{-2} and 65 °C.

With the increase of the EDH concentration, the evolution of Ni surface microstructure was shown in Fig. 1. Without EDH addition, the Ni film was branch-shaped and incompact structure (Fig. 2 (a)). This kind of microstructure was attributed to the nickel chloride and the low current density [16]. When the EDH concentration was 0.3 mol L^{-1}, some flower structures appeared on the Ni branch and the Ni film tended to show oriented growth (Fig. 1 (b)). With the EDH concentration continuously increasing, the finer Ni nanocones took the place of the bigger Ni flowers on the substrate. When the EDH concentration was up to 1.5 mol L^{-1}, only Ni nanocones could be observed on the surface. The density of the nanocones was the highest and the nanocone size was relatively uniform. Oriented growth of Ni nanocones contributed to the EDH which also improved consistency and homogeneity of Ni arrays. However, the EDH solubility was limited; too much EDH addition would lead to precipitation.

Based on the result above, EDH addition could increase the density of Ni nanocones. It was assumed that it might facilitate the nuclei growth process [17]. This hypothesis would be further discussed. Besides, during the electroplating process, oriented growth may depend on the absorption of EDH on specific crystal plane.

In order to investigate the formation mechanism of Ni nanocone arrays, the phase composition and crystal structure were measured by XRD and the result was shown in Fig. 2. Three obvious characteristic peaks were observed. The Bragg reflection peaks at around 45°, 53° and 77° should correspond to the (111), (200) and (220) crystal faces of fcc-Ni (JCPDS Card No. 04-0850). Other peaks were indicated the Cu crystal (JCPDS Card No. 451488). Besides, texture coefficient of plated Ni film could be calculated as follow [18]:

$$TC_{(hkl)} = \frac{I_{(hkl)}/I_{0(hkl)}}{\sum_{i=1}^{n} I_{(hkl)}/I_{0(hkl)}} \times 100\%$$

where $I_{(hkl)}$ and $I_{0(hkl)}$ were diffraction peak intensity of sample and standard Ni flat film respectively. As shown in Table. 1, EDH could restrict the growth of (111) crystal face and facilitate the growth of other two crystal planes by preferential absorption.

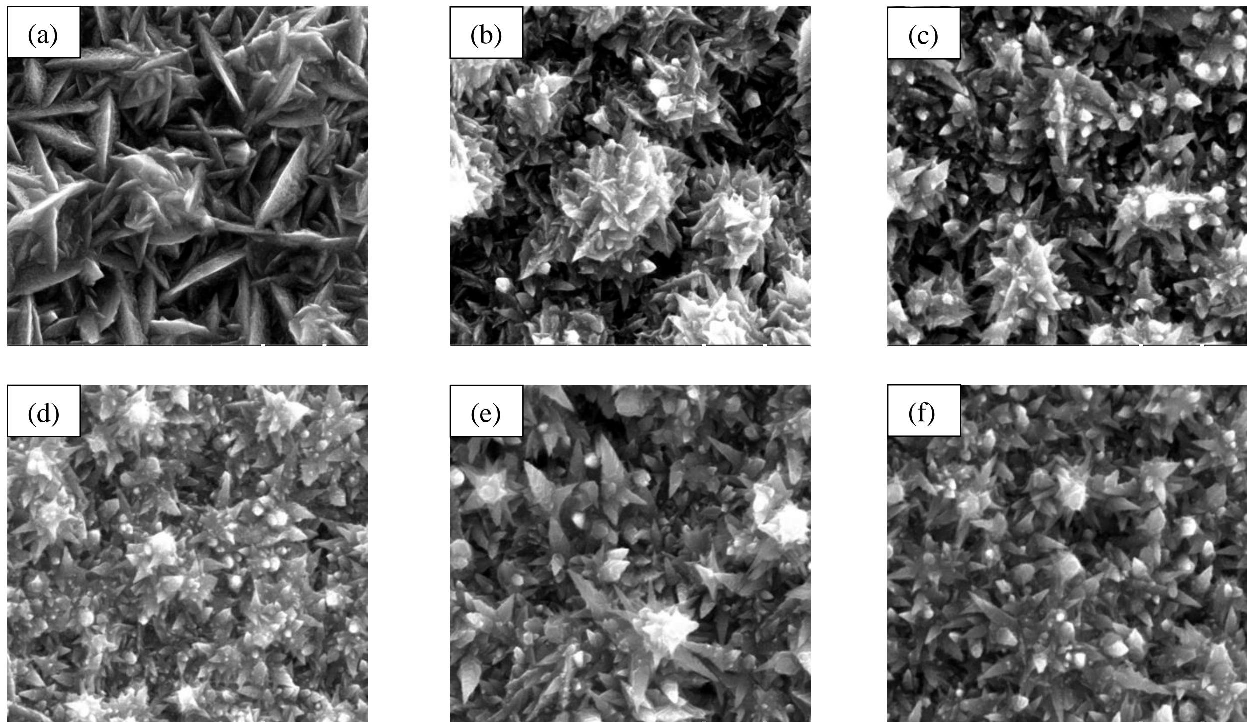

Figure 1. SEM images of Ni film surface with different EDH concentrations (a) 0 mol L^{-1}; (b) 0.3 mol L^{-1}; (c) 0.6 mol L^{-1}; (d) 0.9 mol L^{-1}; (e) 1.2 mol L^{-1}; (f) 1.5 mol L^{-1}. Scale bar, 500 nm.

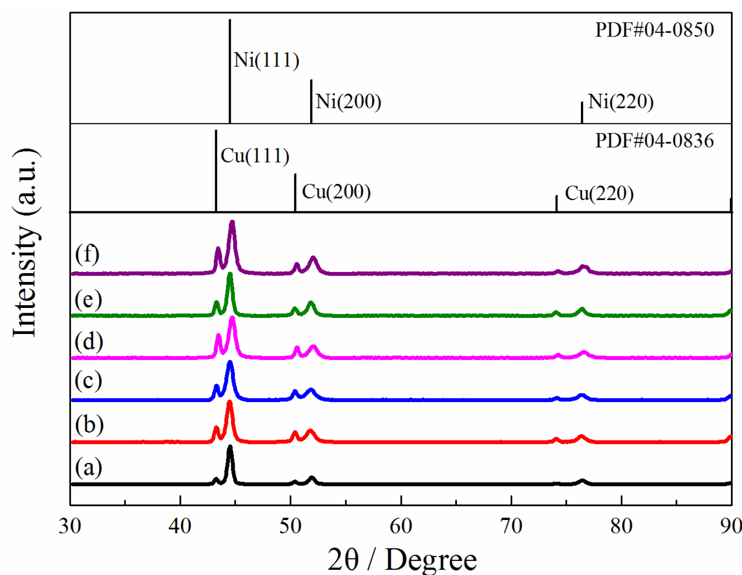

Figure 2. XRD patterns of Ni film with different EDH concentrations (a) 0 mol L^{-1} (b) 0.3 mol L^{-1} (c) 0.6 mol L^{-1} (d) 0.9 mol L^{-1} (e) 1.2 mol L^{-1} (f) 1.5 mol L^{-1}

Table 1. Texture coefficients of plated Ni films with 1.5 mol L^{-1} EDH and without EDH

Crystal plane	*TC* without EDH (%)	*TC* with 1.5 mol L^{-1} EDH (%)
(111)	51.8	40.0
(200)	22.8	30.0
(220)	25.4	30.0

3.2. Electrochemical Behavior of EDH

Ni deposition Linear Sweep Voltammetry curves in different EDH concentrations were shown in Fig. 3. It was found that the current density increased with the increase of EDH concentration at the same overpotential, which indicated a faster reaction rate [19]. During the electroplating process, the EDH would absorb on cathode and release hydrogen ion so that pH value decreased and accelerated the Ni deposition. It was noteworthy that when the overpotential was less than 120 mV, it was hardly to assurance the positive correlation between reaction rate and EDH concentration. In low overpotential zone, the absorption of EDH might hinder the movement of nickel ions and decreased the deposition rate. In high overpotential zone, the steric hindrance effect caused by EDH could be ignored due to the large driving force of reaction and substantial hydrogen evolution on the cathode [20].

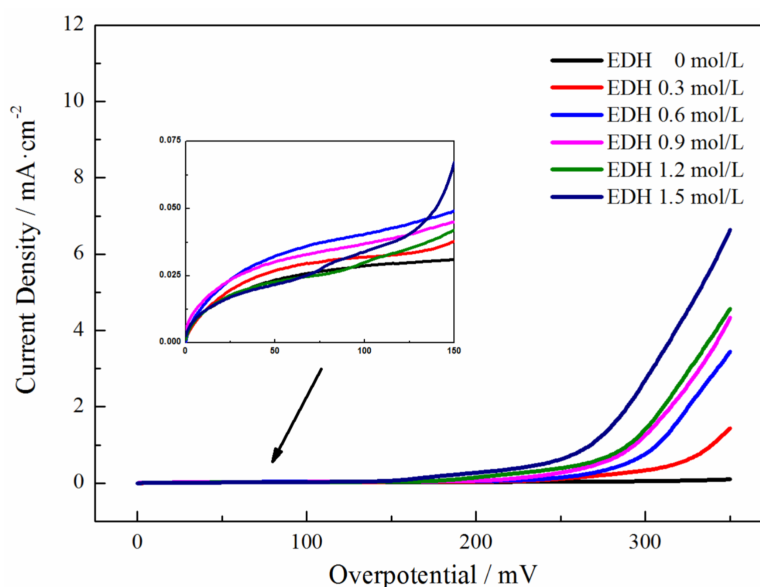

Figure 3. Ni deposition polarization curves with different EDH concentrations

In order to investigate the EDH behavior in the Ni deposition process, the EIS measurements were further carried out. The classic complex plane Nyquist plots were obtained in different EDH concentrations at the same overpotential, as shown in Fig. 4. In order to analyze Ni deposition electrochemical parameters in different EDH concentrations, the measured data were simulated using nonlinear-leastsquare fitting analysis (NLS) software.

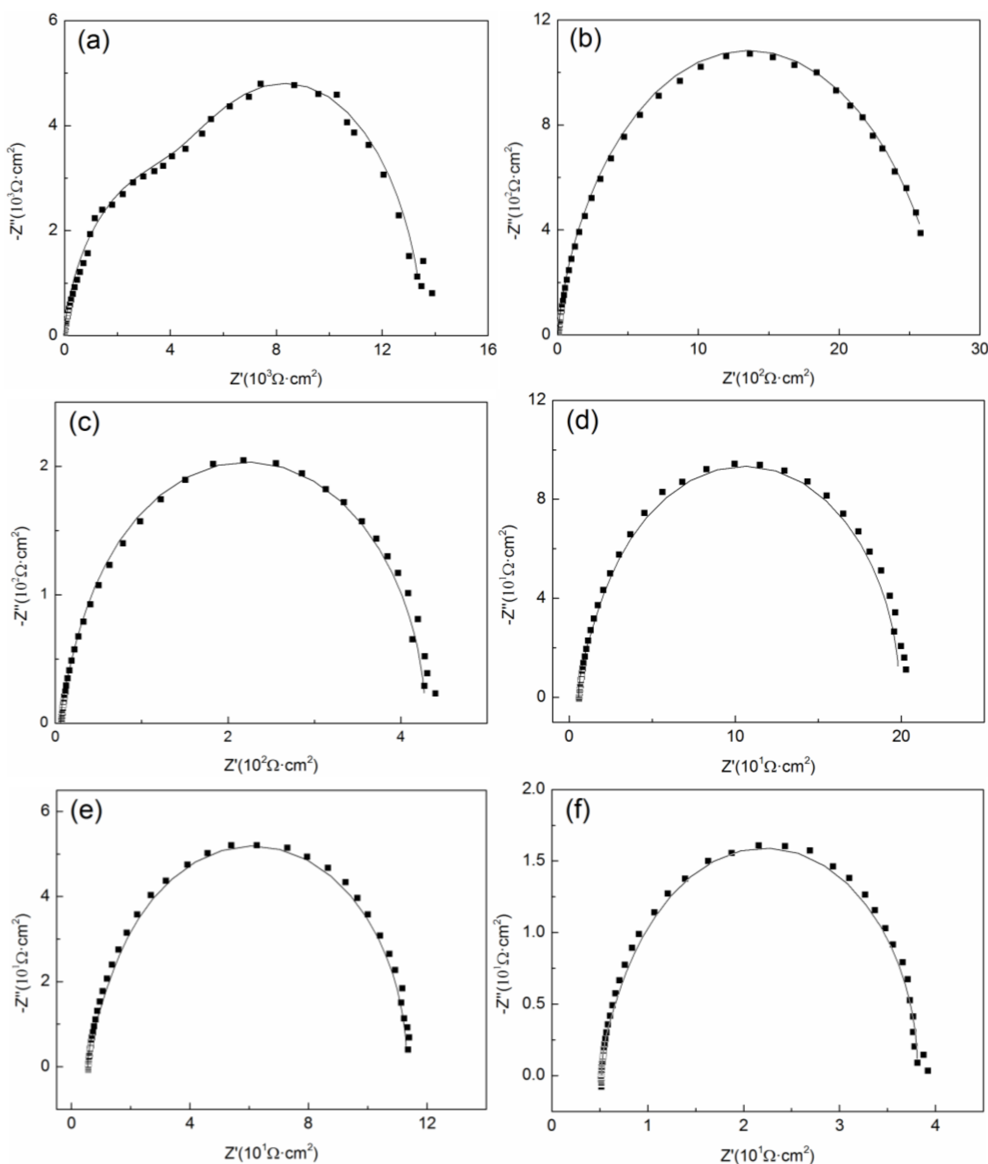

Figure 4. Experimental (symbols) and fitted (solid lines) Nyquist plots for Ni deposition with different EDH concentrations at an overpotential of 250 mV (a) 0 mol L^{-1}; (b) 0.3 mol L^{-1}; (c) 0.6 mol L^{-1}; (d) 0.9 mol L^{-1}; (e) 1.2 mol L^{-1}; (f) 1.5 mol L^{-1}.

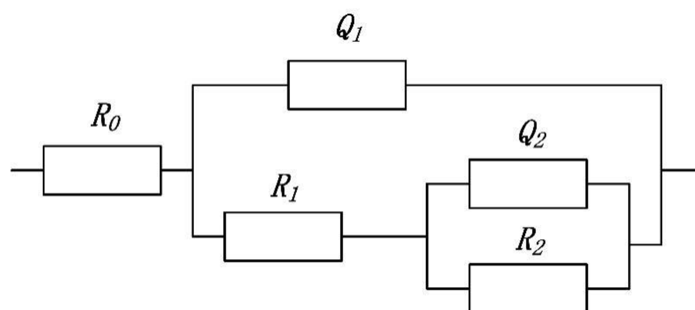

Figure 5. Equivalent circuit used for fitting the impedance results

The electrical circuit model selected to discuss the Ni electrochemical process in different EDH concentrations was shown in Fig. 5, which was similar to elsewhere proposed [21, 22]. In the equivalent

circuit, R_0 is the solution resistance. R_1 is the electrochemical charge transfer resistance. Q_1 is associated with the double layer capacitance (C_{dl}). R_2 is related to the resistance of the adsorbed intermediate compound, and Q_2 is the constant phase element of the pseudo-capacitance.

The fitting result was showed in Table 2. With the increase of EDH concentration, the resistance of Ni deposition process decreased significantly. The result indicated that EDH could facilitate the deposition of nickel and it was in coincident with the polarization curve test.

Table 2. Electrochemical resistance parameters obtained from the EIS measurements

EDH (mol L^{-1})	0	0.3	0.6	0.9	1.2	1.5
R_1 ($\Omega \cdot cm^2$)	7182	1627	146.6	72.09	32.74	14.94

During the Ni nanoarrays electroplating progress, the cathode reaction mechanism could be explained as below: The deposition of nickel was supposed to be accompanied with the hydrogen evolution reaction, which led to the increase of pH value in surface diffusion layer. The enriched OH^- would react with Ni^{2+} to form $Ni(OH)_2$ and absorb on the surface of substrate, which would hinder the electroplating process and increase electrochemical polarization [23]. When EDH was added, EDH could absorb on the plate and promote the acid-base stability in diffusion layer to enhance the diffusion of Ni^{2+}. At the same time, the absorbed EDH hindered the growth of specific crystal plane and facilitated the preferential growth of nickel.

3.3. Temperature and Current density Effect on Nickel Nanocone Arrays

Solution temperature is of great significance to electroplate process [24, 25]. To investigate the influence of temperature, the nickel films were deposited under 0, 30, 45, 60, 75 and 90 °C. The density of nanocone arrays, bottom diameter and consistency were analyzed to evaluate the morphology of nanocone arrays. The Ni array consistency was defined as the standard deviation of the bottom diameter divided by the average of the bottom diameter, which could eliminate the effect of array size difference and evaluate regularity of nanocone arrays. Different temperature Ni film SEM images were showed in Fig. 6 and the evaluation result was listed in Table. 3.

Below 30°C, it was found that the nickel film was flat with cracks, which could be attributed to the layer high internal stress under low temperature. When the temperature was up to 45°C, the Ni nanocone and nanomace structure could be observed, but the overall consistency of the nanostructure was low. The morphology with the good consistency and relatively smaller bottom diameter nanocones appeared at 60°C. Continuing increasing the temperature, the nanocone bottom diameter would grow bigger and the nanocone density would decrease. In the low temperature zones, the diffusion rate of the nickel ions was extremely slow and concentration polarization increased, it was difficult to get nanoarray structure [26]. In the relatively high temperature zones, the higher diffusion rate of the nickel ions decreased the concentration polarization, and the nickel nanocone arrays were formed.

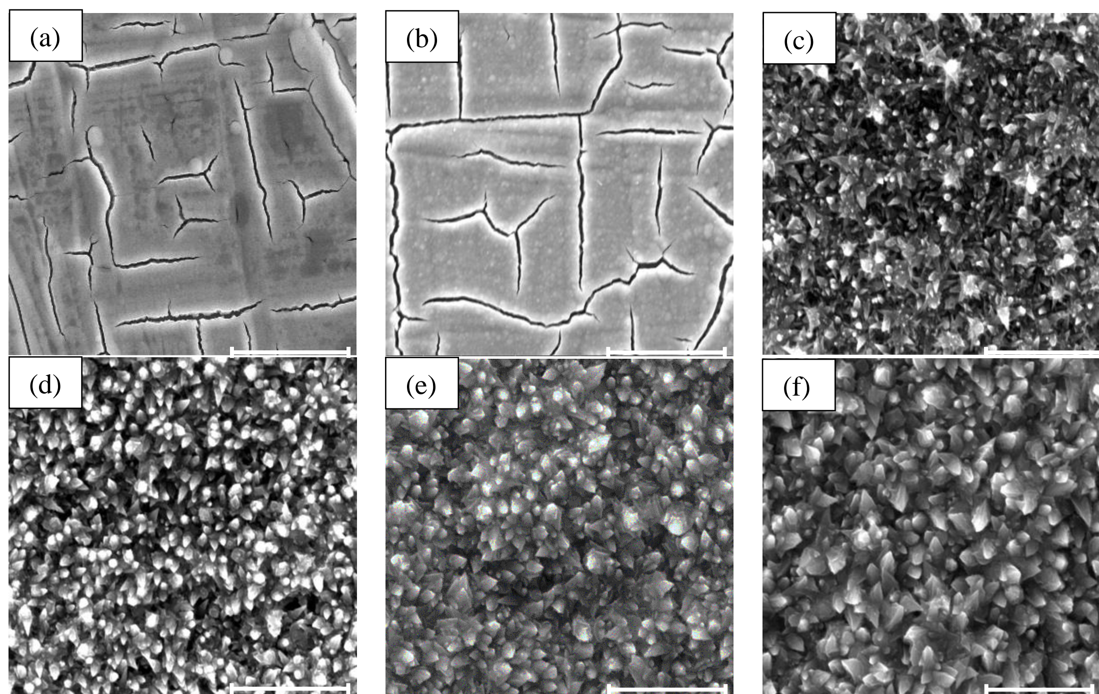

Figure 6. SEM images of Ni film surface under different temperature (a) 0 ℃ (b) 30 ℃ (c) 45 ℃ (d) 60℃ (e) 75℃ (f) 90℃. Scale bar, 2 μm.

Table 3. Array density and consistency under different temperature

Temperature (°C)	Array density (10^8 cm^{-2})	Bottom diameter (nm)	Standard deviation	Consistency
45	19.75	130	41.01	0.3155
60	18.25	150	25.90	0.1727
75	12.75	190	48.63	0.2559
90	9.64	240	57.90	0.2413

The current density played a vital role in the formation of nickel nanocone arrays [27, 28]. To investigate current density effect, nickel films were deposited at the current density of 0.5, 1.0, 1.5, 2.0, 2.5 and 3.0 A dm^{-2}. According to the Ferrari's first law, the amount of electric quantity was proportional to the mass of deposited layer. In order to obtain the same thickness, electroplating time were set as 480, 240, 160, 120, 96 and 80 s. The SEM images of Ni films at different current densities were showed in Fig. 7. Due to the disordered morphology at large current density, only the films deposited at 0.5 and 1.0 A dm^{-2} were evaluated and the results were listed in Table. 4.

The nanocone arrays were relatively uniform and consistent at the low current density (< 1.5 A dm^{-2}). When the current density was up to 1.5 A dm^{-2}, the nanomace structure was formed. In contrast to the Ni grain growth, the Ni nucleation process was promoted at higher overpotential [29]. New nanocone could nucleate and grow on the preformed nanocone and form the nanomace. The formed nanomace exhibited an irregular morphology. Therefore, it was selected 1.0 A dm^{-2} as the deposition parameter to form the nanocones. The electrodeposition process was usually divided into two parts, nucleation and growth [30]. When the current density was 1.0 A dm^{-2}, the reduced Ni atoms nucleated

and formed the nanocones, which was the dominant process. When the current density continually increased, the higher overpotentical would facilitate the nucleation, and accelerate the nanomace structure formation.

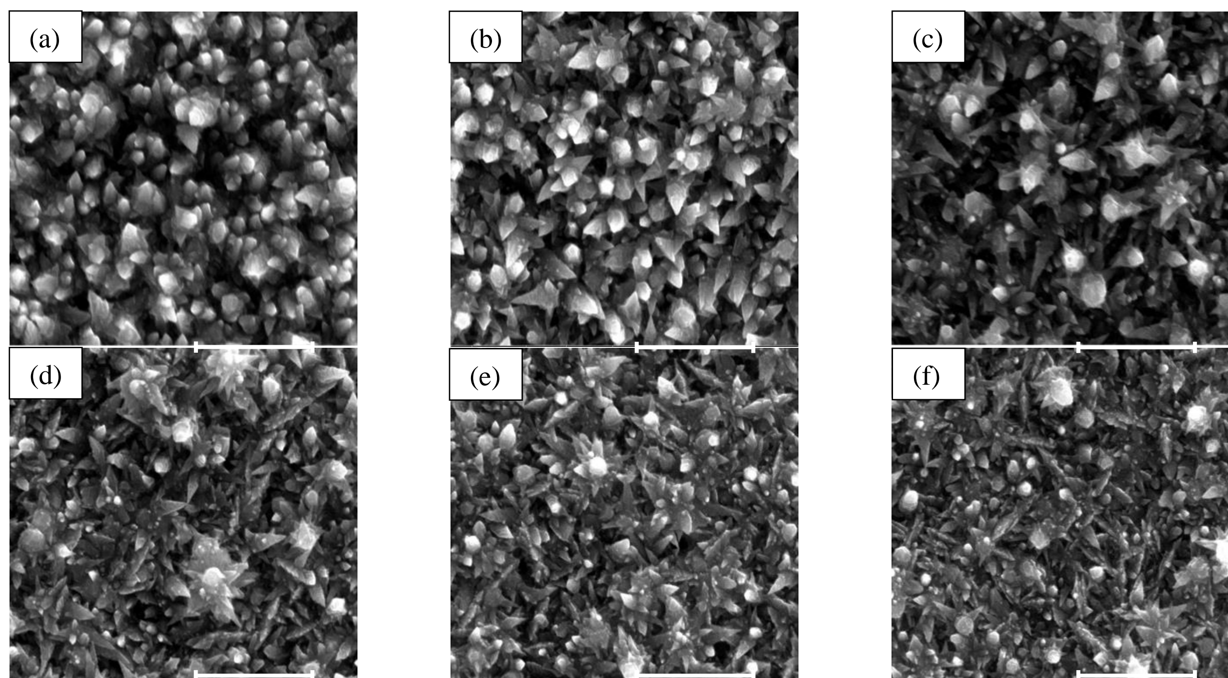

Figure 7. SEM images of Ni film surface at different current density (a) 0.5 A dm^{-2} (b) 1.0 A dm^{-2} (c) 1.5 A dm^{-2} (d) 2.0 A dm^{-2} (e) 2.5 A dm^{-2} (f) 3.0 A dm^{-2}. *Scale bar, 1 μm.*

Table 4. Array density and consistency at different current density

Current density (A dm^{-2})	Array density (10^8 cm^{-2})	Bottom diameter (nm)	Standard deviation	Consistency
0.5	11.75	140	39.05	0.2789
1.0	18.25	150	25.90	0.1727

3.4. Effect of Nanostructure on Joint Strength and Interface

Nickel-coated pad was susceptible to the oxidation which imposed a threat to the reliability of interconnection joint. Immersion gold was commonly selected as surface finishing to prevent surface oxidation and enhance wetting ability [31, 32]. After the nickel deposition, gold was immersion plated on the nickel film. The surface morphology of Ni/Au layer was showed in Fig. 8. It was suggested that the nanocone morphology was kept after the Au coated. The silver nanoparticles were observed by TEM. As showed in Fig. 9, the mean size of silver nanoparticles was about 20 nm. The Ag nanoparticles dispersed well without obvious aggregation. The as-prepared Ag NPs were dispersed in the deionized water under ultrasound treatment for 30 min, and then centrifuged at 3500 rpm for 5 min. The resulting precipitates were redispersed in deionized water to prepare the paste [15].

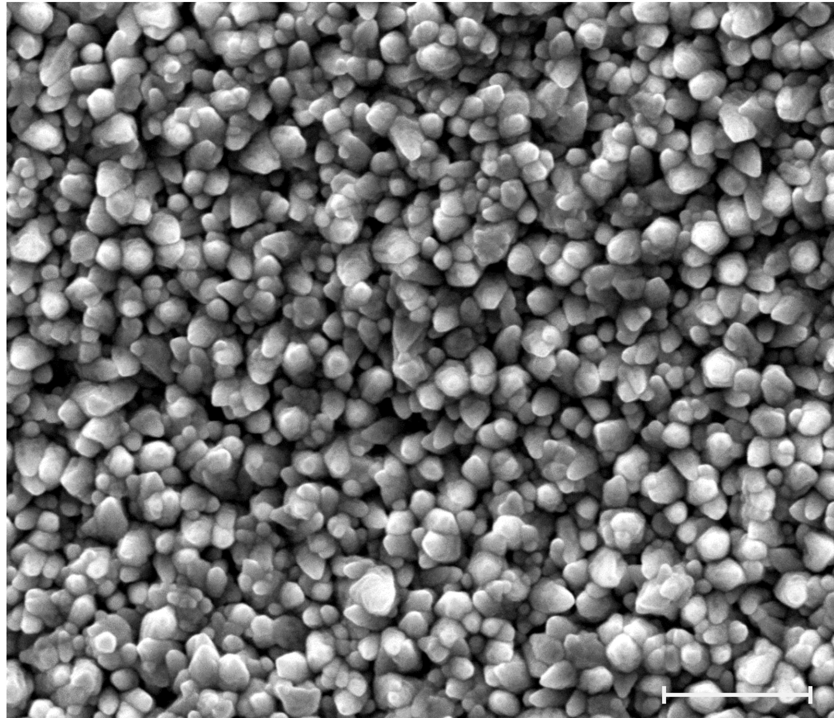

Figure 8. SEM image of the Ni/Au nanoarray surface. *Scale bar, 2 μm.*

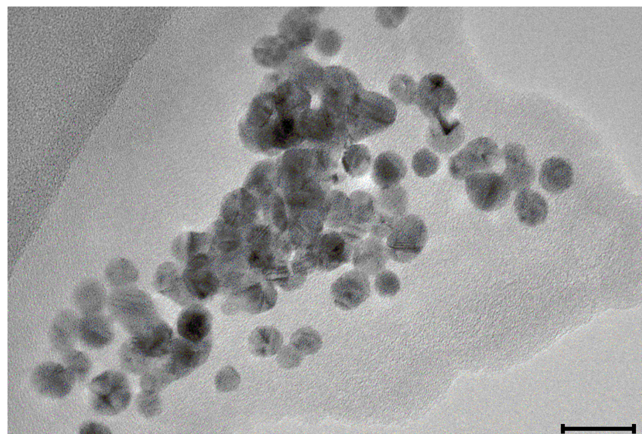

Figure 9. TEM image of Ag nanoparticles. *Scale bar, 20 nm.*

The shear strengths of joints with different nanocone bottom diameters were listed in Fig. 10. The nanostructure contributed significantly to the enhancement of shear strength compared with the flat pad joints. When the nanocone bottom diameter was 150 nm, the joint held the best shear strength. It was indicated that the surface nanostructure could enhance the joint performance, and the compatibility between nano paste and pad was influenced by the microstructures of them. The matched surface energy between the surface nano arrays and the Ag NP paste should be the essential factor in the sinter process. In this study, the 150 nm nanoarrays showed the best-fit to 20 nm Ag NP paste, too large or small nano array diameters may make the surface energy mismatch.

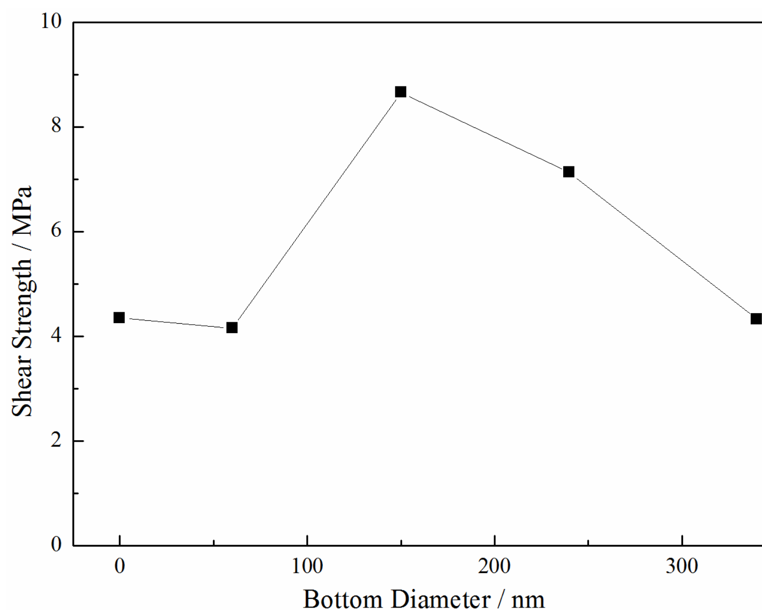

Figure 10. Shear strength of Ni/Au nano-array film with different bottom diameter

4. CONCLUSIONS

In summary, we had successfully fabricated Ni/Au nanocone arrays on the Cu pad surface. The EDH effect on the Ni deposition was analyzed. The electrochemical test results showed the EDH could decrease the polarization, and promoted the nanostructure formation. The plating parameters, such as temperature and current density, were tuned by the Ni array density and bottom diameter. The Ni/Au nanocone arrays were sintered with Ag nanopaste. The results showed the surface nanostructure could enhance the joint shear strength. The reinforced effect depended on the nanocone bottom diameter.

ACKNOWLEDGMENTS
The authors thank for the support by the National Nature Science Foundation of China (grant numbers 51505104, 2015 and grant numbers 51608155, 2016) and China Postdoctoral Science Foundation under grant 2014M561344.

References

1. J. Millán, P. Godignon, X. Perpiñà, A. Pérez-Tomás and J. Rebollo, *IEEE T. Power Electr.,* 29 (2014) 2155.
2. A.Q. Huang, *Proc. IEEE*, 105 (2017) 2019.
3. D. Nakamura, I. Gunjishima, S. Yamaguchi, T. Ito, A. Okamoto, H. Kondo, Onda S. and K. Takatori, *Nature*, 430 (2004) 1009.
4. S.H. Mannan and M.P. Clode, *IEEE Trans. Adv. Pack.*, 27 (2004) 508.
5. S. Kim, K.S. Kim, S.S. Kim and K. Suganuma, *J. Electron. Mater.*, 38 (2009) 266.
6. C. Chen, H.M. Tong and K.N. Tu, *Annu. Rev. Mater. Res.*, 40 (2010) 531.
7. E. Breckenfeld, H. Kim, R.C.Y. Auyeung, N. Charipar, P. Serra and A. Piqué, *Appl. Surf. Sci.*, 331

(2015) 254.
8. K.S. Tan, Y.H. Wong and K.Y. Cheong, *Int. J. Therm. Sci.,* 87 (2015) 169.
9. X. Liu, Z. Zheng, C. Wang, W. Liu, R. An and W. Zhang, *J. Mater. Sci. Mater. Electron.*, 28 (2017) 8206.
10. Y. Zhong, R. An, C. Wang, Z. Zheng, Z.Q. Liu, C.H. Liu, C.F. Li, T.K. Kim and S.H. Jin, *Small*, 11 (2015) 4097.
11. S. Wang, M. Li, H. Ji and C. Wang, *Scripta Mater.*, 69 (2013) 789.
12. J. Liu, H. Chen, H. Ji and M. Li, *ACS Appl. Mater. Inter.*, 8 (2016) 33289.
13. H. Alarifi, A. Hu, M. Yavuz and Y.N. Zhou, *J. Electron. Mater.*, 40 (2011) 1394.
14. W. Zhou, Z. Zheng, C. Wang, Z. Wang and R. An, *ACS Appl. Mater. Inter.*, 9 (2017) 4798.
15. M. Li, Y. Xiao, Z. Zhang and J. Yu, *ACS Appl. Mater. Inter.*, 7 (2015) 9157.
16. Y. Yang, *Int. J. Electrochem. Sci.*, 10 (2015) 5164.
17. Y. Yu, L. Sun, H. Ge, G. Wei and L. Jiang, *Int. J. Electrochem. Sci.*, 12 (2017) 485.
18. Z. Zheng, N. Li, C.Q. Wang, D.Y. Li, Y.M. Zhu and G. Wu, *Int. J. Hydrogen Energ.*, 37 (2012) 13921.
19. D. Hou, W. Zhou, X. Liu, K. Zhou, J. Xie, G. Li and S. Chen, *Electrochim. Acta,* 166 (2015) 26.
20. E.S. Güler, E. Konca and İ. Karakaya, *Int. J. Electrochem. Sci.*, 8 (2013) 5496.
21. J.N. Balaraju, V.E. Selvi, V.W. Grips and K.S. Rajam, *Electrochim. Acta*, 52 (2006) 1064.
22. C.E. Davalos, J.R. Lopez, H. Ruiz, A. Méndez, R. Antano-Lopez and G. Trejo, *Int. J. Electrochem. Sci.*, 8 (2013) 9785.
23. B. Ash, K.G. Mishra, T. Subbaiah, R.K. Paramguru and B.K. Mishra, *J. Power Sources*, 275 (2015) 55.
24. O.K. Al-Duaij, M.M. Abou-Krisha and M.I. Attia, *Int. J. Electrochem. Sci.*, 12 (2017) 11972.
25. J.P. Hou, Y. Bai, C.W. Su and J.M. Guo, *Int. J. Electrochem. Sci.*, 10 (2015) 10576.
26. X. Zhou and Y. Shen, *Appl. Surf. Sci.*, 324 (2015) 677.
27. J. Kang, I. Ryu, G. Choe, G. Kim and S. Yim, *Int. J. Electrochem. Sci.*, 12 (2017) 9588.
28. W. Lu, P. Huang, C. He and B. Yan, *Int. J. Electrochem. Sci.*, 8 (2013) 914.
29. M. Palomar-Pardavé, J. Aldana-González, L.E. Botello, E.M. Arce-Estrada, M.T. Ramírez-Silva, J. Mostany and M. Romero-Romo, *Electrochim. Acta*, 241 (2017) 162.
30. X. Yang-tao, D. Yu-jie, Z. Wei and X. Tian-dong, *Surf. Coating Technol.*, 330 (2017) 170.
31. H.R. Kotadia, P.D. Howes and S.H. Mannan, *Microelectron. Reliab.*, 54 (2014) 1253.
32. H. Qi, S. Ganesan and M. Pecht, *Microelectron. Reliab.*, 48 (2008) 663.

© 2020 The Authors. Published by ESG (www.electrochemsci.org). This article is an open access article distributed under the terms and conditions of the Creative Commons Attribution license (http://creativecommons.org/licenses/by/4.0/).